8

Experimental Control of Flexible Robot Manipulators

A. Sanz and V. Etxebarria
Universidad del País Vasco
Spain

1. Introduction

Flexible-link robotic manipulators are mechanical devices whose control can be rather challenging, among other reasons because of their intrinsic under-actuated nature. This chapter presents various experimental studies of diverse robust control schemes for this kind of robotic arms. The proposed designs are based on several control strategies with well defined theoretical foundations whose effectiveness are demonstrated in laboratory experiments.

First it is experimented a simple control method for trajectory tracking which exploits the two-time scale nature of the flexible part and the rigid part of the dynamic equations of flexible-link robotic manipulators: a slow subsystem associated with the rigid motion dynamics and a fast subsystem associated with the flexible link dynamics. Two experimental approaches are considered. In a first test an LQR optimal design strategy is used, while a second design is based on a sliding-mode scheme. Experimental results on a laboratory two-dof flexible manipulator show that this composite approach achieves good closed-loop tracking properties for both design philosophies, which compare favorably with conventional rigid robot control schemes.

Next the chapter explores the application of an energy-based control design methodology (the so-called IDA-PBC, interconnection and damping assignment passivity-based control) to a single-link flexible robotic arm. It is shown that the method is well suited to handle this kind of under-actuated devices not only from a theoretical viewpoint but also in practice. A Lyapunov analysis of the closed-loop system stability is given and the design performance is illustrated by means of a set of simulations and laboratory control experiments, comparing the results with those obtained using conventional control schemes for mechanical manipulators.

The outline of the chapter is as follows. Section 2 covers a review on the modeling of flexible-link manipulators. In subsection 2.1 the dynamic modelling of a general flexible multilink manipulator is presented and in subsection 2.2 the methodology is applied to a laboratory flexible arm. Next, some control methodologies are outlined in section 3. Two control strategies are applied to a two-dof flexible robot manipulator. The first design, in subsection 3.1, is based on an optimal LQR approach and the second design, in subsection 3.2, is based on a sliding-mode controller for the slow subsystem. Finally, section 4 covers the IDA-PBC method. In subsection 4.1 an outline of the method is given and in subsection

4.2 the proposed control strategy based on IDA-PBC is applied to a laboratory arm. The chapter ends with some concluding remarks.

2. Modeling of flexible-link manipulator

2.1 The dynamic modeling of a general flexible multilink manipulator

In order to obtain a dynamic model for a multilink flexible robot manipulator, it becomes necessary the introduction of a convenient kinematic description of the manipulator, including the deformation of the links. In order to limit the complexity of the derivation, it is assumed that rigid motion and link deformation happen in the same plane, without torsional effects. A sketch of a two-link manipulator of this kind is shown in Fig. 1 with an appropriate coordinate frame assignment.

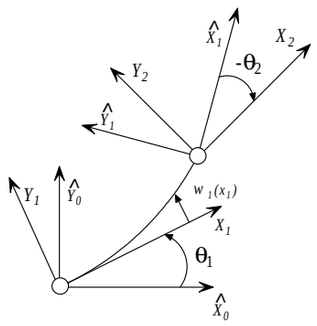

Figure 1. Planar two-link flexible manipulator

The rigid motion is described by the joint angles θ_1, θ_2, while $w_1(x_1)$ denotes the transversal deflection of link 1 at x_1 with $0 \leq x_1 \leq l_1$, being l_1 the link length. This deflection is expressed as a superposition of a finite number of modes where the spatial and time variables are separated:

$$w_1(x,t) = \sum_{i=1}^{n_e} \varphi_i(x) q_i(t) \tag{1}$$

where $\varphi_i(x)$ is the mode shape and $q_i(t)$ is the mode amplitude.

To obtain a finite-dimensional dynamic model, the assumed modes link approximation can be used. By applying Lagrange's formulation the dynamics of any multilink flexible-link robot can be represented by

$$H(r)\ddot{r} + V(r,\dot{r}) + Kr + F(\dot{r}) + G(r) = B(r)\tau \tag{2}$$

where r(t) expresses the position vector as a function of the rigid variables θ and the deflection variables q. $H(r)$ represents the inertia matrix, $V(r,\dot{r})$ are the components of the Coriolis vector and centrifugal forces, K is the diagonal and positive definite link stiffness matrix, $F(\dot{r})$ is the friction matrix, and $G(r)$ is the gravity matrix. $B(r)$ is the input matrix, which depends on the particular boundary conditions corresponding to the assumed modes. Finally, τ is the vector of the input joint torques.

The explicit equations of motion can be derived computing the kinetic energy T and the potential energy U of the system and then forming the Lagrangian.

The kinetic energy of the entire system is

$$T = \sum_{i=1}^{n} T_{hi} + \sum_{i=1}^{n} T_{li} \tag{3}$$

where T_{hi} is the kinetic energy of the rigid body located at hub i of mass m_{hi} and moment of inertia I_{hi}; r_i indicates the absolute position in frame $(\hat{X}_0, \hat{Y}_0)$ of the origin of frame (X_i, Y_i) and $\dot{\alpha}_i$ is the absolute angular velocity of frame (X_i, Y_i).

$$T_{hi} = \frac{1}{2} m_{hi} \dot{r}_i^T \dot{r}_i + \frac{1}{2} I_{hi} \dot{\alpha}_i^2 \tag{4}$$

And T_{li} is the kinetic energy of the *ith* element where ρ_i is the mass density per unit length of the element and $\dot{p}_i$ is the absolute linear velocity of an arm point.

$$T_{li} = \frac{1}{2} \int_0^{li} \rho_i(x_i) \dot{p}_i(x_i)^T \dot{p}_i(x_i) dx_i \tag{5}$$

Since the robot moves in the horizontal plane, the potential energy is given by the elastic energy of the system, because the gravitational effects are supported by the structure itself, and therefore they disappear inside the formulation:

$$U = \sum_{i=1}^{n} U_{ei} \tag{6}$$

The elastic energy stored in link i is

$$U_{ei} = \frac{1}{2} \int (EI)_i(x_i) \left(\frac{d^2 w_i(x_i)}{dx_i^2}\right)^2 dx_i \tag{7}$$

The total elastic energy of the system can be written as:

$$U = U_e = \frac{1}{2} q^T \cdot K \cdot q \tag{8}$$

where K is the diagonal stiffness matrix that only affects to the flexible modes.
As a result, the dynamical equation (2) can be partitioned in terms of the rigid, $\theta_i(t)$, and flexible, $q_{ij}(t)$, generalized coordinates.

$$\begin{pmatrix} H_{\theta\theta}(\theta,q) & H_{\theta q}(\theta,q) \\ H_{\theta q}^T(\theta,q) & H_{qq}(\theta,q) \end{pmatrix} \begin{pmatrix} \ddot{\theta} \\ \ddot{q} \end{pmatrix} + \begin{pmatrix} c_\theta(\theta,q,\dot{\theta},\dot{q}) \\ c_q(\theta,q,\dot{\theta},\dot{q}) \end{pmatrix} + \begin{pmatrix} 0 \\ D\dot{q} + Kq \end{pmatrix} = \begin{pmatrix} \tau \\ 0 \end{pmatrix} \tag{9}$$

Where $H_{\theta\theta}$, $H_{\theta q}$ y H_{qq} are the blocks of the inertia matrix H, which is symmetric and positive definite, c_θ, c_q are the components of the vector of Coriolis and centrifugal forces and D is the diagonal and positive semidefinite link damping matrix.

2.2 Application to a flexible laboratory arm

The above analysis will now be applied to the flexible manipulator shown in Fig. 2, whose geometric sketch is displayed in Fig. 3. As seen in the figures, it is a laboratory robot which

moves in the horizontal plane with a workspace similar to that of common Scara industrial manipulators. Links marked 1 and 4 are flexible and the remaining ones are rigid. The flexible links' deflections are measured by strain gauges, and the two motor's positions are measured by standard optical encoders.

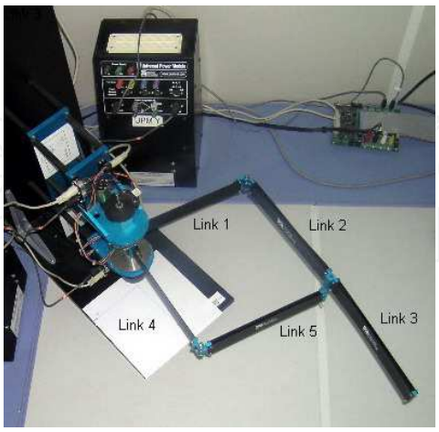

Figure 2. Photograph of the experimental flexible manipulator

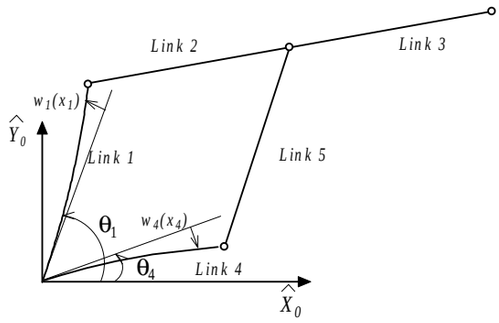

Figure 3. Planar two-dof flexible manipulator

The model is obtained by a standard Lagrangian procedure, where the inertia matrices have the structure:

$$H_{\theta\theta}(\theta,q)=\begin{pmatrix} h_{11} & h_{12} \\ h_{21} & h_{22} \end{pmatrix} \quad H_{\theta q}(\theta,q)=\begin{pmatrix} h_{13} & h_{14} \\ h_{23} & h_{24} \end{pmatrix} \quad H_{qq}(\theta,q)=\begin{pmatrix} h_{33} & h_{34} \\ h_{43} & h_{44} \end{pmatrix}$$

with:

$$\begin{aligned} h_{11} = \; & I_{h1} + m_{j1}(l^2 + \varphi_1^2 q_1^2) + m_{j2}(2l^2 + \varphi_1^2 q_1^2 + l^2 \varphi_4'^2 q_4^2) + I_{h5} + I_{h6} + \frac{1}{3} m_1 l^2 + \varsigma_{111} q_1^2 + m_2(2l^2 + 2\varphi_1^2 q_1^2) \\ & + m_5\left(\frac{1}{3} l^2 + \frac{1}{3} l^2 \varphi_4'^2 q_4^2\right) \\ h_{12} = \; & m_{j2}(2l^2 \cos(\theta_1 - \theta_4) + l^2 \varphi_1'^2 q_1 \sin(\theta_1 - \theta_4) - l\varphi_1 q_1 \sin(\theta_1 - \theta_4) + l\cos(\theta_1 - \theta_4)\varphi_1 \varphi_1' q_1^2 - l^2 \sin(\theta_1 - \theta_4)\varphi_4' q_4 \\ & + l\sin(\theta_1 - \theta_4)\varphi_4 q_4 + l\cos(\theta_1 - \theta_4)\varphi_4 \varphi_4' q_4^2) + 2m_2(l^2 \cos(\theta_1 - \theta_4) + l^2 \sin(\theta_1 - \theta_4)\varphi_1' q_1 - l\sin(\theta_1 - \theta_4)\varphi_1 q_1 \\ & + l\cos(\theta_1 - \theta_4)\varphi_1 \varphi_1' q_1^2) + m_5\left(\frac{1}{2} l^2 \cos(\theta_1 - \theta_4) - \frac{1}{2} l^2 \sin(\theta_1 - \theta_4)\varphi_4' q_4 + \frac{1}{2} l \sin(\theta_1 - \theta_4)\varphi_4 q_4 \right. \\ & \left. + \frac{1}{2} l \cos(\theta_1 - \theta_4)\varphi_4 \varphi_4' q_4^2\right) \end{aligned}$$

$$h_{21} = h_{12}$$

$$h_{22} = I_{h2} + m_{j2}(l^2 + l^2\varphi_1'^2 q_1^2) + I_{h3} + I_{h4} + m_{j1}(l^2 + \varphi_4^2 q_4^2) + m_{j2}(l^2 + \varphi_4^2 q_4^2) + 2m_2(\frac{4}{3}l^2 + \frac{4}{3}l^2\varphi_1'^2 q_1^2) + \frac{1}{3}m_4 l^2 + \varsigma_{411} q_4^2 + m_5(l^2 + \varphi_4^2 q_4^2)$$

$$h_{13} = m_{j1} l\varphi_1 + m_{j2}(l\varphi_1 + l^2\cos(\theta_1 - \theta_4)\varphi_1' - l\sin(\theta_1 - \theta_4)\varphi_1\varphi_1' q_1) + \upsilon_{11} + 2m_2(l\varphi_1 + l^2\cos(\theta_1 - \theta_4)\varphi_1' - l\sin(\theta_1 - \theta_4)\varphi_1\varphi_1' q_1)$$

$$h_{14} = I_{h5}\varphi_4' + m_{j2}(l^2\varphi_4' + l\cos(\theta_1 - \theta_4)\varphi_4 - l\sin(\theta_1 - \theta_4)\varphi_4\varphi_4' q_4) + I_{h6}\varphi_4' + m_5(\frac{1}{3}l^2\varphi_4' - \frac{1}{2}l\sin(\theta_1 - \theta_4)\varphi_4\varphi_4' q_4 + \frac{1}{2}l\cos(\theta_1 - \theta_4)\varphi_4)$$

$$h_{23} = \begin{aligned} & I_{h2}\varphi_1' + m_{j2}(l^2\varphi_1' + l\cos(\theta_1 - \theta_4)\varphi_1 + l\sin(\theta_1 - \theta_4)\varphi_1\varphi_1' q_1) \\ & + I_{h3}\varphi_1' + 2m_2(\frac{4}{3}l^2\varphi_1' + l\sin(\theta_1 - \theta_4)\varphi_1\varphi_1' q_1 \\ & + l\cos(\theta_1 - \theta_4)\varphi_1) \end{aligned}$$

$$h_{24} = m_{j1} l\varphi_4 + m_{j2}(l\varphi_4 + l^2\cos(\theta_1 - \theta_4)\varphi_4' + l\sin(\theta_1 - \theta_4)\varphi_4\varphi_4' q_4) + \upsilon_{41} + m_5(l\varphi_4 + \frac{1}{2}l^2\cos(\theta_1 - \theta_4)\varphi_4' + \frac{1}{2}l\sin(\theta_1 - \theta_4)\varphi_4\varphi_4' q_4)$$

$$h_{33} = m_{j1}\varphi_1^2 + I_{h2}\varphi_1'^2 + m_{j2}(\varphi_1^2 + l^2\varphi_1'^2 + 2l\cos(\theta_1 - \theta_4)\varphi_1\varphi_1') + I_{h3}\varphi_1'^2 + \varsigma_{111} + 2m_2(\varphi_1^2 + \frac{4}{3}l^2\varphi_1'^2 + 2l\cos(\theta_1 - \theta_4)\varphi_1\varphi_1')$$

$$h_{34} = h_{43} = 0$$

$$h_{44} = m_{j1}\varphi_4^2 + I_{h5}\varphi_4'^2 + m_{j2}(\varphi_4^2 + l^2\varphi_4'^2 + 2l\cos(\theta_1 - \theta_4)\varphi_4\varphi_4') + I_{h6}\varphi_4'^2 + \varsigma_{411} + m_5(\varphi_4^2 + \frac{1}{3}l^2\varphi_4'^2 + l\cos(\theta_1 - \theta_4)\varphi_4\varphi_4')$$

where φ_i is the amplitude of the first mode evaluated in the end of the link i, $\varphi_i' = (d\varphi_i / dx_i)\big|_{x_i = l_i}$; υ_{ij} is the deformation moment of order one of mode j of link i and ς_{ijk} is the cross moment of modes j and k of link i. Also l is the links length, m_{j1} is the elbow joint mass, m_{j2} is the tip joint mass, m_i (i=1,4) is the flexible link mass, m_k (k=2,3,5) is the rigid link mass and q_i is the deflection variable.

3. Control design

The control of a manipulator formed by flexible elements bears the study of the robot's structural flexibilities. The control objective is to move the manipulator within a specific trajectory but attenuating the vibrations due to the elasticity of some of its components.
Since time scales are usually present in the motion of a flexible manipulator, it can be considered that the dynamics of the system is divided in two parts: one associated to the manipulator's movement, considered slow, and another one associated to the deformation of the flexible links, much quicker. Taking advantage of this separation, diverse control strategies can be designed.

3.1 LQR control design

In a first attempt to design a control law, a standard LQR optimal technique is employed. The error feedback matrix gains are obtained such that the control law $\tau(t) = -K_c \Delta x$ minimizes the cost function:

$$J = \int_0^\infty (\Delta x^* Q \Delta x + \tau * R\tau) dt \tag{10}$$

where Q and R are the standard LQR weighting matrices; and Δx is the applicable state vector comprising either flexible, rigid or both kind of variables. This implies to minimize the tracking error in the state variables, but with an acceptable cost in the control effort. The resulting Riccati equations can conveniently be solved with state-of-the-art tools such as the Matlab Control System Toolbox .

The effectiveness of the proposed control schemes has been tested by means of real time experiments on a laboratory two-dof flexible robot. This manipulator, fabricated by Quanser Consulting Inc. (Ontario, Canada), has two flexible links joined to rigid links using high quality low friction joints. The laboratory system is shown in Fig. 2.

From the general equation (9) the dynamics corresponding to the rigid part can be extracted:

$$\begin{pmatrix} h_{11}(\theta,q) & h_{12}(\theta,q) \\ h_{21}(\theta,q) & h_{22}(\theta,q) \end{pmatrix} \begin{pmatrix} \ddot{\theta}_1 \\ \ddot{\theta}_4 \end{pmatrix} + \begin{pmatrix} c_{11}(\theta,q,\dot{\theta},\dot{q}) \\ c_{21}(\theta,q,\dot{\theta},\dot{q}) \end{pmatrix} = \begin{pmatrix} \tau_1 \\ \tau_4 \end{pmatrix} \tag{11}$$

The first step is to linearize the system (11) around the desired final configuration or reference configuration. Defining the incremental variable $\Delta\theta = \theta - \theta_d$ and with a state-space representation defined by $\Delta x = (\Delta\theta \quad \Delta\dot{\theta})^T$ the approximate model corresponding to the considered flexible manipulator's rigid part can be described as:

$$\Delta\dot{x} = \begin{pmatrix} 0 & 0 & 1 & 0 \\ 0 & 0 & 0 & 1 \\ 0 & 0 & 0 & 0 \\ 0 & 0 & 0 & 0 \end{pmatrix} \Delta x - \begin{pmatrix} 0 \\ H_{\theta\theta}^{-1} \end{pmatrix} \tau \tag{12}$$

where it has been taken into account the fact that the Coriolis terms are zero around the desired reference configuration.

Table 1 displays the physical parameters of the laboratory robot. Using these values, the following control laws have been designed. In all the experiments the control goal is to follow a prescribed cartesian trajectory while damping the excited vibrations as much as possible.

Property	Value
Motor 1 inertia , I_h	0.0081 Kgm^2
Link length, l	0.23 m
Flexible link mass, m_1,m_4	0.09 Kg
Rigid link mass, m_2,m_3,m_5	0.08 Kg
Elbow joint mass, m_{j1}	0.03 Kg
Tip joint mass, m_{j2}	0.04 Kg

Table 1. Flexible link parameters

The control goal is to track a cartesian trajectory which comprises 10 straight segments in about 12 seconds. Each stretch is covered in approximately 0.6 seconds, after which the arm remains still for the same time at the points marked 1 to 10 in Fig. 4. As a first test, Fig. 5 shows the system's response with a pure rigid LQR controller that is obtained solving the Riccati equations for R=*diag* (2 2) and Q=*diag*(20000 20000 10 10). The values of R and Q have been chosen experimentally, keeping in mind that if the values of Q are relatively large with respect to the values of R a quick evolution is specified toward the desired equilibrium $\Delta x = 0$ which causes a bigger control cost (see (10)). As seen in the figures, this kind of control, which is very commonly used for rigid manipulators, is able to follow the prescribed trajectory but with a certain error, due to the links' flexibilities.
It has been shown in the above test that, as expected, a flexible manipulator can not be very accurately controlled if a pure rigid control strategy is applied. From now on two composite control schemes (where both the rigid and the flexible dynamics are taken into account) will be described.
The non-linear dynamic system (9) is being linearized around the desired final configuration. The obtained model is:

$$\begin{pmatrix} H_{\theta\theta}(\theta,q) & H_{\theta q}(\theta,q) \\ H_{\theta q}^{T}(\theta,q) & H_{qq}(\theta,q) \end{pmatrix} \begin{pmatrix} \Delta\ddot{\theta} \\ \Delta\ddot{q} \end{pmatrix} + \begin{pmatrix} 0 & 0 \\ 0 & K \end{pmatrix} \begin{pmatrix} \Delta\theta \\ \Delta q \end{pmatrix} = \begin{pmatrix} \Delta\tau \\ 0 \end{pmatrix} \tag{13}$$

where again the Coriolis terms are zero around the given point.
Reducing the model to the maximum (taking a single elastic mode in each one of the flexible links), a state vector is defined as:

$$\Delta x = (\Delta\theta \quad \Delta q \quad \Delta\dot{\theta} \quad \Delta\dot{q})^{T} \tag{14}$$

and the approximate model of the considered flexible manipulator can be described as:

$$\Delta\dot{x} = \begin{pmatrix} 0 & 0 & I & 0 \\ 0 & 0 & 0 & I \\ 0 & L_2^{-1}H_{qq}^{-1}K & 0 & 0 \\ 0 & L_1^{-1}H_{\theta q}^{T-1}K & 0 & 0 \end{pmatrix} \Delta x + \begin{pmatrix} 0 \\ 0 \\ L_2^{-1}H_{\theta q}^{-1} \\ L_1^{-1}H_{\theta\theta}^{-1} \end{pmatrix} \Delta\tau \tag{15}$$

where

$$L_1^{-1} = (H_{\theta\theta}^{-1}H_{\theta q} - H_{\theta q}^{T-1}H_{qq})^{-1}$$
$$L_2^{-1} = (H_{\theta q}^{-1}H_{\theta\theta} - H_{qq}^{-1}H_{\theta q}^{T})^{-1}$$

Following the same LQR control strategy as in the previous lines, a scheme is developed making use of the values of Table 1, with R=*diag*(2 2) and Q=*diag*(19000 19000 1000000 1000 100 100 100 100). From measurements on the laboratory robot the following values for the elements' inertias I_{h2} =I_{h3} =I_{h5} =I_{h6} =1.10^{-5} Kg.m^2 have been estimated. Also the elastic constant K=113, and the space form in the considered vibration modes φ_{11}= φ_{41}=0.001m and φ'_{11}= φ'_{41} =0.1 have been measured.

In Fig. 6 the obtained results applying a combined LQR control are shown. The tip position exhibits better tracking of the desired trajectory, as it can be seen comparing Fig. 5(a) and Fig. 6(a). Even more important, it should be noted that the oscillations of elastic modes are now attenuated quickly (compare Fig. 5(b,c) and Fig. 6(b,c)).

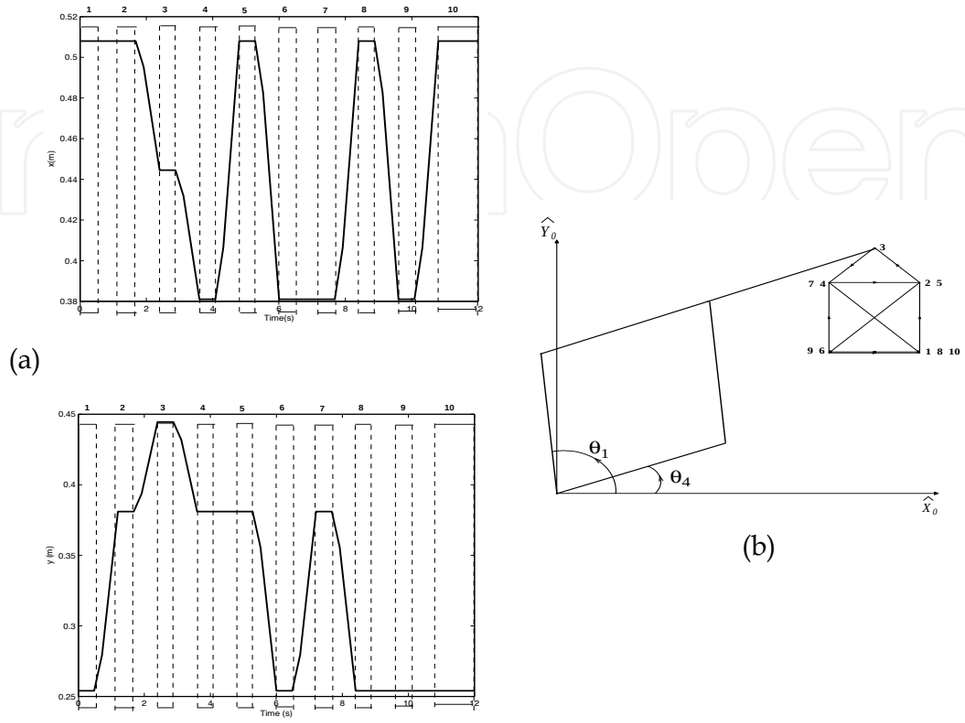

Figure 4. Cartesian trajectory of the manipulator. (a) Time evolution of the x and y coordinates. (b) Sketch of the manipulator and trajectory

3.2 Sliding-mode control design

The presence of unmodelled dynamics and disturbances can lead to poor or unstable control performance. For this reason the rigid part of the control can be designed using a robust sliding mode philosophy, instead of the previous LQR methods. This control design has been proved to hold solid stability and robustness theoretical properties in rigid manipulators (Barambones & Etxebarria, 2000), and is tested now in real experiments.
The rigid control law is thus changed to:

$$\tau_{ri} = \begin{cases} p_i \cdot \mathrm{sgn}(S_i) & if \quad |S_i| > \beta_i \\ p_i \dfrac{S_i}{\beta_i} & otherwise \end{cases}$$

where $\beta = (\beta_1, \ldots, \beta_n)^T, \beta_i > 0$ is the width of the band for each sliding surface associated to each motor, p_i is a constant parameter and S is a surface vector defined by $S = \dot{E} + \lambda E$, being $E = \theta - \theta_d$ the tracking error (θ_d is the desired trajectory vector) and $\lambda = diag(\lambda_1, \ldots, \lambda_n), \lambda_i > 0$.

The philosophy of this control is to attract the system to S_i=0 by an energetic control $p \cdot \mathrm{sgn}(S_i)$ and once inside a band around S_i=0, to regulate the position using a smoother control, roughly coincident with the one designed previously. The sliding control can be tuned by means of the sliding gain p and by adjusting the width of band β which limits the area of entrance of the energetic part of the control. It should be kept in mind that the external action to the band should not be excessive, to avoid exciting the flexibilities of the fast subsystem as much as possible (which would invalidate the separation hypothesis between the slow dynamics and the fast one).

In this third experiment a second composite control scheme (sliding-mode for the slow part and LQR for the fast one) is tested.

Fig. 7 exhibits the experimental results obtained with the sliding control strategy described for the values β=(6 4 9 4) and λ=(10.64 6.89 32.13 12.19). β is the width of the band for each sliding surface associated to each motor, which limits the area of entrance of the energetic part of the control. If the values of β are too big, the action of the energetic control is almost negligible; on the contrary if this values are too small, the action of the external control is much bigger and the flexible modes can get excited. The width of the band is chosen by means of a trial-and-error experimental methodology. The values used of λ are such that the gain control values inside the band match the LQR gains designed in the previous section.

In the same way as with the combined LQR control, the rigid variable follows the desired trajectory, and again, the elastic modes are attenuated with respect to the rigid control, (compare Fig. 5(b,c) and Fig. 7(b,c)). Also, it can be seen that this attenuation is even better than in the previous combined LQR control case (compare Fig. 6(b,c) and Fig. 7(b,c)).

To gain some insight on the differences of the two proposed combined schemes, the contribution to the control torque is compared in the sliding-mode case (rigid) with the LQR combined control case (rigid), both to τ_1 (Fig. 8(a) and 8(b)). It is observed how in the intervals from 1 to 2s., 2 to 3s. (corresponding to the stretch between the points marked 2 and 3 in Fig.4) and 7 to 8s. (corresponding to the diagonal segment between the points marked 7 and 8 in Fig.4), the sliding control acts in a more energetic fashion, favoring this way the pursuit of the wanted trajectory. However, in the intervals from 5 to 6s. (point marked 5 in Fig.4), 6 to 7s. (marked 6), 9.5 to 10.5s. (marked 9) and 11 to 12s. (marked 10), in the case of the sliding control, a smoother control acts, and its control effort is smaller than in the case of the LQR combined control, causing this way smaller excitation of the oscillations in these intervals (as it can be seen comparing Fig. 7(b,c) with Fig. 6(b,c)). Note that the sliding control should be carefully tuned to achieve its objective (attract the system to S_i =0) but without introducing too much control activity which could excite the flexible modes to an unwanted extent.

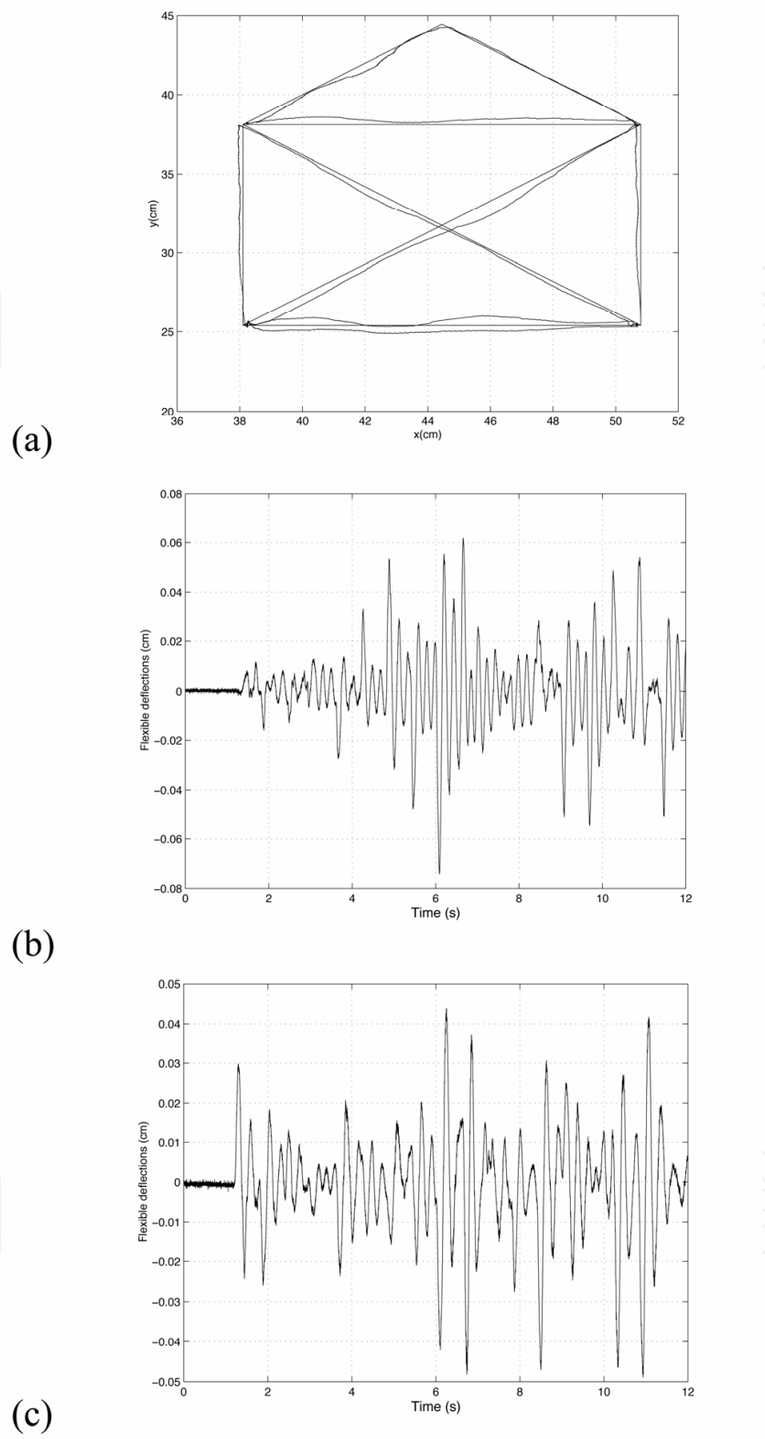

Figure 5. Experimental results for pure rigid LQR control. a) Tip trajectory and reference. b) Time evolution of the flexible deflections (link 1 deflections). c) Time evolution of the flexible deflections (link 4 deflections)

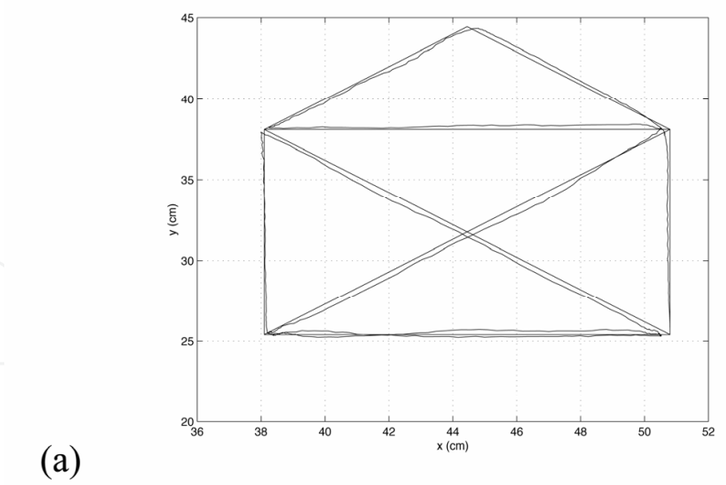

(a)

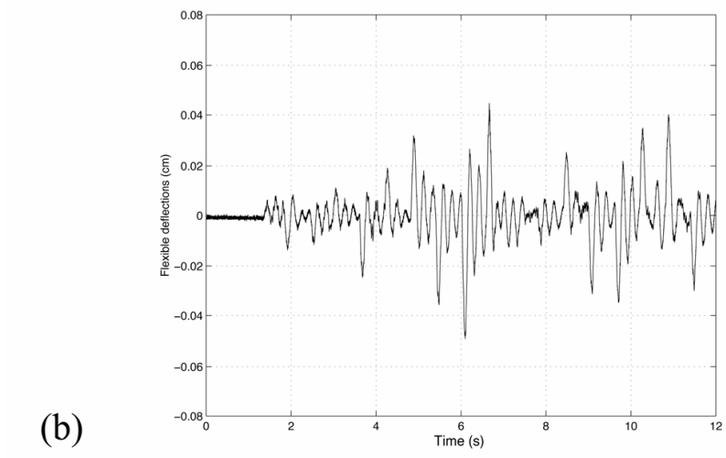

(b)

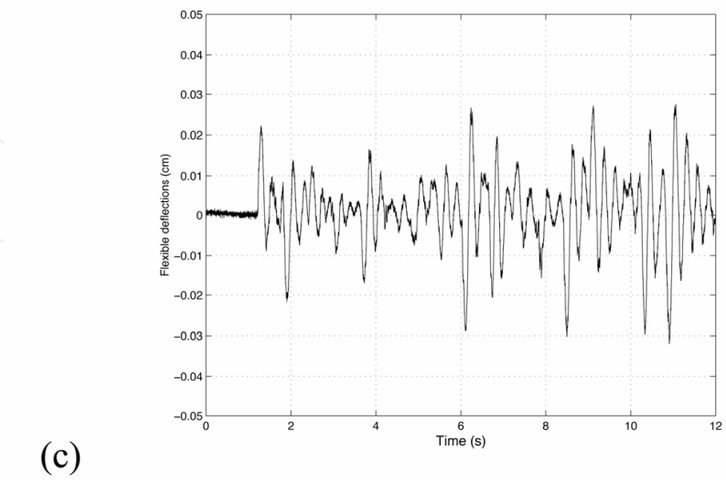

(c)

Figure 6. Experimental results for composite (slow-fast) LQR control. a) Tip trajectory and reference. b) Time evolution of the flexible deflections (link 1 deflections). c) Time evolution of the flexible deflections (link 4 deflections)

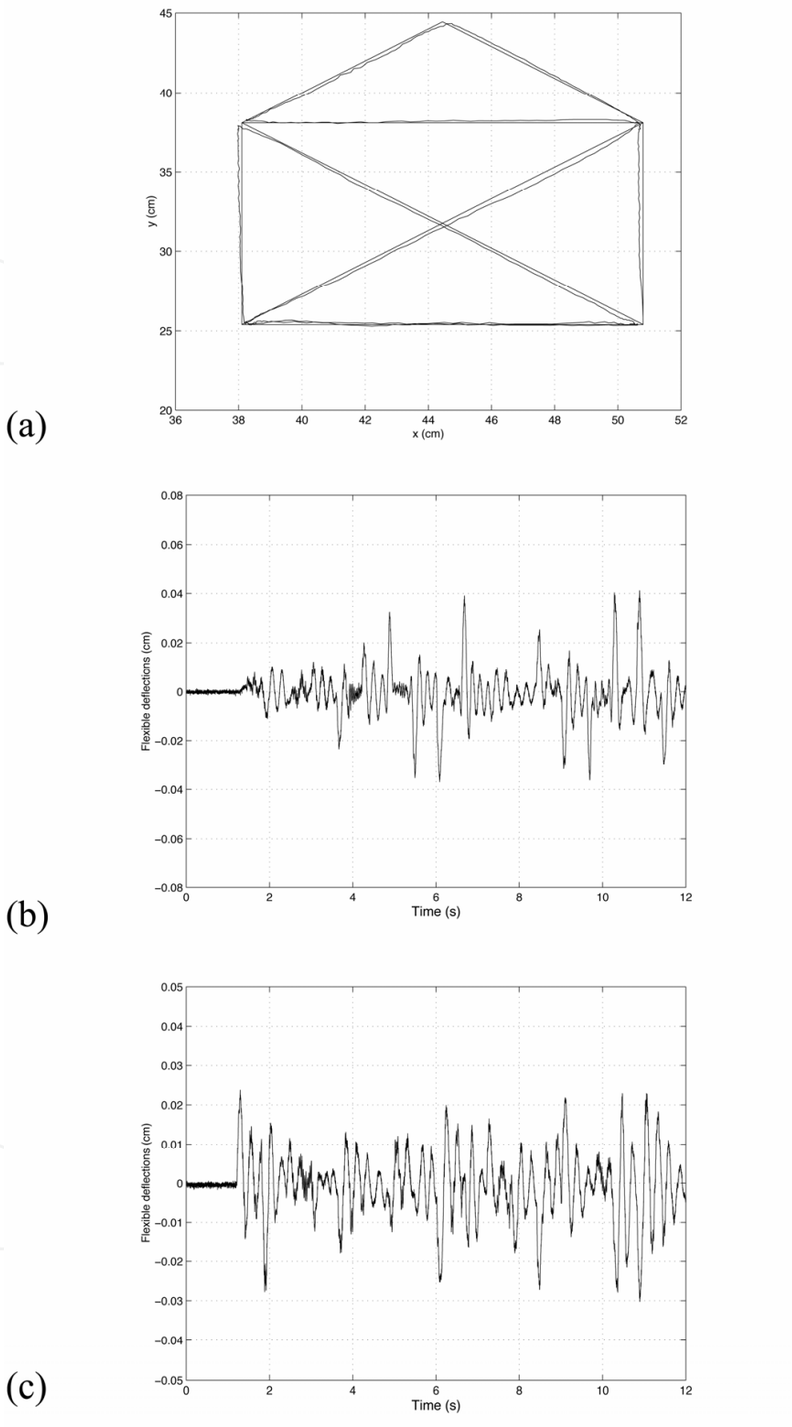

Figure 7. Experimental results for composite (slow-fast) sliding-LQR control. a) Tip trajectory and reference. b) Time evolution of the flexible deflections (link 1 deflections). c) Time evolution of the flexible deflections (link 4 deflections)

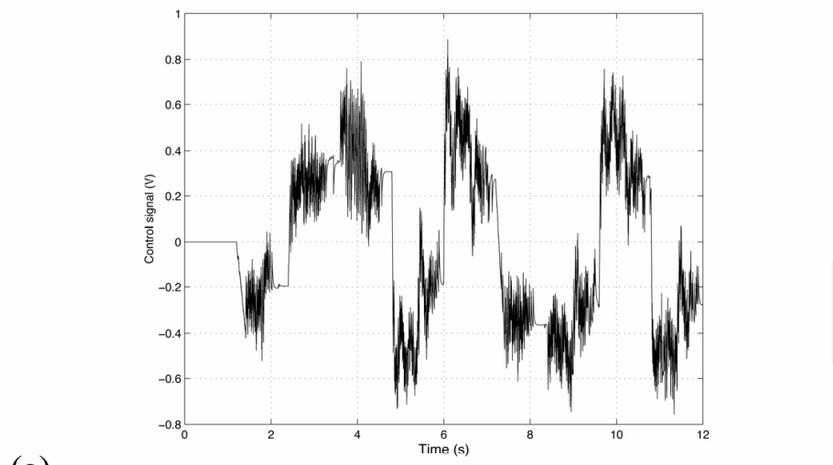

(a)

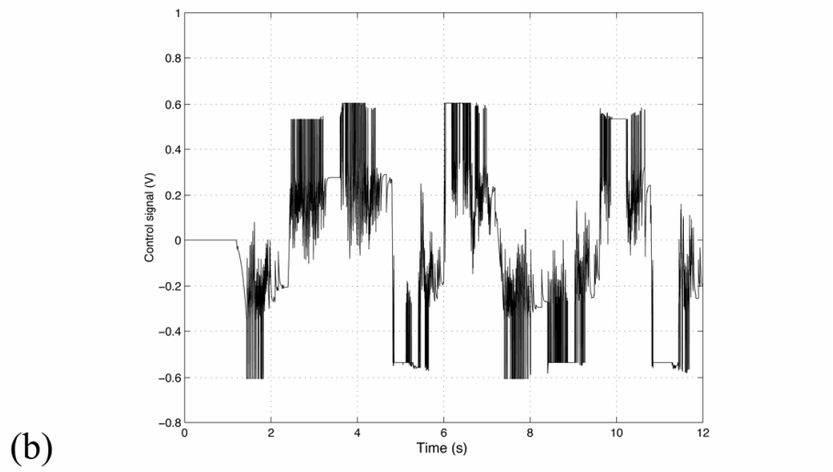

(b)

Figure 8. a) Contribution to the torque control τ_1 (rigid) with the LQR combined control squeme. b) Contribution to the torque control τ_1 (rigid) in the sliding-mode case

4. The IDA-PBC method

4.1 Outline of the method

The IDA-PBC (interconnection and damping assignment passivity-based control) method is an energy-based approach to control design (see (Ortega & Spong, 2000) and (Ortega et al., 2002) for complete details). The method is specially well suited for mechatronic applications, among others. In the case of a flexible manipulator the goal is to control the position of an under-actuated mechanical system with total energy:

$$H(q,p) = \frac{1}{2} p^T M^{-1}(q) p + U(q) \tag{16}$$

where $q \in \mathbb{R}^n$, $p \in \mathbb{R}^n$, are the generalized positions and momenta respectively, $M(q)=M^T(q)>0$ is the inertia matrix and U(q) is the potential energy.

If it is assumed that the system has no natural damping, then the equations of motion of such system can be written as:

$$\begin{pmatrix} q \\ p \end{pmatrix} = \begin{pmatrix} 0 & I_n \\ -I_n & 0 \end{pmatrix} \begin{pmatrix} \nabla_q H \\ \nabla_p H \end{pmatrix} + \begin{pmatrix} 0 \\ G(q) \end{pmatrix} u \tag{17}$$

The IDA-PBC method follows two basic steps:

1. Energy shaping, where the total energy function of the system is modified so that a predefined energy value is assigned to the desired equilibrium.
2. Damping injection, to achieve asymptotic stability.

The following form for the desired (closed-loop) energy function is proposed:

$$H_d(q,p) = \frac{1}{2} p^T M_d^{-1}(q) p + U_d(q) \tag{18}$$

where $M_d = M_d^T > 0$ is the closed-loop inertia matrix and U_d the potential energy function.

It will be required that U_d have an isolated minimum at the equilibrium point q_*, that is:

$$q_* = \arg\min \quad U_d(q) \tag{19}$$

In PBC, a composite control law is defined:

$$u = u_{es}(q,p) + u_{di}(q,p) \tag{20}$$

where the first term is designed to achieve the energy shaping and the second one injects the damping.

The desired (closed-loop) dynamics can be expressed in the following form:

$$\begin{pmatrix} \dot{q} \\ \dot{p} \end{pmatrix} = \left(J_d(q,p) - R_d(q,p) \right) \begin{pmatrix} \nabla_q H_d \\ \nabla_p H_d \end{pmatrix} \tag{21}$$

where

$$J_d = -J_d^T = \begin{pmatrix} 0 & M^{-1} M_d \\ -M_d M^{-1} & J_2(q,p) \end{pmatrix} \tag{22}$$

$$R_d = R_d^T = \begin{pmatrix} 0 & 0 \\ 0 & G K_v G^T \end{pmatrix} \geq 0 \tag{23}$$

represent the desired interconnection and damping structures. J_2 is a skew-symmetric matrix, and can be used as free parameter in order to achieve the kinetic energy shaping (see Ortega & Spong, 2000)).

The second term in (20) , the damping injection, can be expressed as:

$$u_{di} = -K_v G^T \nabla_p H_d \tag{24}$$

where $K_v = K_v^T > 0$.

To obtain the energy shaping term u_{es} of the controller, (20) and (24), the composite control law, are replaced in the system dynamic equation (17) and this is equated to the desired closed-loop dynamics, (21):

$$\begin{pmatrix} 0 & I_n \\ -I_n & 0 \end{pmatrix}\begin{pmatrix} \nabla_q H \\ \nabla_p H \end{pmatrix}+\begin{pmatrix} 0 \\ G \end{pmatrix}u_{es}=\begin{pmatrix} 0 & M^{-1}M_d \\ -M_d M^{-1} & J_2(q,p) \end{pmatrix}\begin{pmatrix} \nabla_q H_d \\ \nabla_p H_d \end{pmatrix}$$

$$Gu_{es}=\nabla_q H - M_d M^{-1}\nabla_q H_d + J_2 M_d^{-1} p \tag{25}$$

In the under-actuated case, G is not invertible, but only full column rank. Thus, multiplying (25) by the left annihilator of G, $G^{\perp}G=0$, it is obtained:

$$G^{\perp}\left\{\nabla_q H - M_d M^{-1}\nabla_q H_d + J_2 M_d^{-1} p\right\}=0 \tag{26}$$

If a solution (M_d,U_d) exists for this differential equation, then u_{es} will be expressed as:

$$u_{es}=(G^T G)^{-1}G^T(\nabla_q H - M_d M^{-1}\nabla_q H_d + J_2 M_d^{-1} p) \tag{27}$$

The PDE (26) can be separated in terms corresponding to the kinetic and the potential energies:

$$G^{\perp}\left\{\nabla_q (p^T M^{-1} p) - M_d M^{-1}\nabla_q (p^T M_d^{-1} p) + 2J_2 M_d^{-1} p\right\}=0 \tag{28}$$

$$G^{\perp}\left\{\nabla_q U - M_d M^{-1}\nabla_q U_d\right\}=0 \tag{29}$$

So the main difficulty of the method is in solving the nonlinear PDE corresponding to the kinetic energy (28). Once the closed-loop inertia matrix, M_d, is known, then it is easier to obtain U_d of the linear PDE (29), corresponding to the potential energy.

4.2 Application to a laboratory arm

The object of the study is a flexible arm with one degree of freedom that accomplishes the conditions of Euler-Bernoulli (Fig.9). In this case, the elastic deformation of the arm w(x,t) can be represented by means of an overlapping of the spatial and temporary parts, see equation (1).

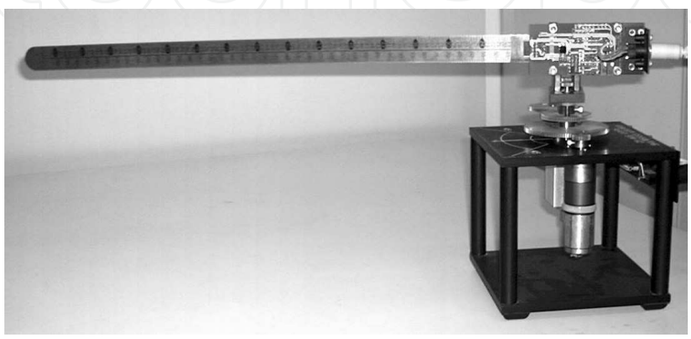

Figure 9. Photograph of the experimental flexible manipulator

If a finite number of modes m is considered, Lagrange equations lead to a dynamical system defined by m+1 second order differential equations:

$$\begin{pmatrix} I_t & 0 \\ 0 & I \end{pmatrix}\begin{pmatrix} \ddot{q}_0(t) \\ \ddot{q}_i(t) \end{pmatrix}+\begin{pmatrix} 0 & 0 \\ 0 & K_f \end{pmatrix}\begin{pmatrix} q_0(t) \\ q_i(t) \end{pmatrix}=\begin{pmatrix} 1 \\ \varphi'(0) \end{pmatrix}u \tag{30}$$

where q_0 (a 1x1 vector) and q_i (an mx1 vector) are the dynamic variables; $q_0(t)$ is the rigid generalized coordinate, $q_i(t)$ is the vector of flexible modes, I_t is the total inertia, K_f is the stiffness mxm matrix that depends on the elasticity of the arm, and it is defined as K_f=diag(ω_i^2), where ω_i is the resonance frequency of each mode; φ' are the first spatial derivatives of $\varphi_i(x)$ evaluated at the base of the robot. Finally u includes the applied control torques. Defining the incremental variables as $\tilde{q} = q - q_d$, where q_d is the desired trajectory for the robot such that $\dot{q}_{0d} \neq 0$, $\ddot{q}_{0d} = 0$ and q_{id}=0, then the dynamical model is given by:

$$\begin{pmatrix} I_t & 0 \\ 0 & I \end{pmatrix}\begin{pmatrix} \ddot{\tilde{q}}_0(t) \\ \ddot{\tilde{q}}_i(t) \end{pmatrix}+\begin{pmatrix} 0 & 0 \\ 0 & K_f \end{pmatrix}\begin{pmatrix} \tilde{q}_0(t)+q_{0d} \\ \tilde{q}_i(t) \end{pmatrix}=\begin{pmatrix} 1 \\ \varphi'(0) \end{pmatrix}u \tag{31}$$

The total energy of the mechanical system is obtained as the sum of the kinetic and potential energy:

$$H(\tilde{q},p)=\frac{1}{2}p^T M^{-1}p+\frac{1}{2}\tilde{q}^T K\tilde{q} \tag{32}$$

where $p=(I_t\dot{\tilde{q}}_0 \quad I\dot{\tilde{q}}_i)^T$ and M and K are (m+1)x(m+1) matrices

$$M=\begin{pmatrix} I_t & 0 \\ 0 & I \end{pmatrix} \quad K=\begin{pmatrix} 0 & 0 \\ 0 & K_f \end{pmatrix}$$

The point of interest is $\tilde{q}_* = (0,0)$, which corresponds to zero tracking error in the rigid variable and null deflections.

The controller design will be made in two steps; first, we will obtain a feedback of the state that produces energy shaping in closed-loop to stabilize the position globally, then it will be injected the necessary damping to achieve the asymptotic stability by means of the negative feedback of the passive output.

The inertia matrix, M, that characterizes to the system, is independent of $\tilde{q}$, hence it follows that it can be chosen J_2=0, (see (Ortega & Spong, 2000)). Then, from (28) it is deduced that the matrix M_d should also be constant. The resulting representation capturing the first flexible mode is

$$M_d=\begin{pmatrix} a_1 & a_2 \\ a_2 & a_3 \end{pmatrix}$$

where the condition of positive definiteness of the inertia matrix, lead to the following inequations:

$$a_1 > 0 \quad a_1 a_3 > a_2^2 \tag{33}$$

Now, considering only the first flexible mode, equation (29) corresponding to the potential energy can be written as:

$$\left(\frac{a_2-\varphi'(0)a_1}{I_t}\right)\frac{\partial U_d}{\partial \tilde{q}_0}+(a_3-\varphi'(0)a_2)\frac{\partial U_d}{\partial \tilde{q}_1}=\tilde{q}_1\omega_1^2 \tag{34}$$

where $\tilde{q}_0=q_0-q_{0d}$ is the rigid incremental variable and $\tilde{q}_1=q_1-0$ is the flexible incremental variable. The equation (34) is a trivial linear PDE whose general solution is

$$U_d=-\frac{I_t^2\omega_1^2(a_3-\varphi'(0)a_2)}{2(-a_2+\varphi'(0)a_1)^2}\tilde{q}_0^2-\frac{I_t\omega_1^2}{(-a_2+\varphi'(0)a_1)}\tilde{q}_0\tilde{q}_1+F(z) \tag{35}$$

$$z=\gamma\tilde{q}_0+\tilde{q}_1 \tag{36}$$

$$\gamma=\frac{I_t(a_3-\varphi'(0)a_2)}{(-a_2+\varphi'(0)a_1)} \tag{37}$$

where F is an arbitrary differentiable function that we should choose to satisfy condition (19) in the points q_*.
Some simple calculations show that the necessary restriction $\nabla_q U_d(0)=0$ is satisfied if $\nabla F(z(0))=0$, while condition $\nabla_q^2 U_d(0)>0$ is satisfied if:

$$F''>\frac{\omega_1^2}{(a_3-\varphi'(0)a_2)} \tag{38}$$

Under these restrictions it can be proposed $F(z)=(1/2)K_1z^2$, with $K_1>0$, which produces the condition:

$$a_3>\varphi'(0)a_2 \tag{39}$$

So now, the term corresponding to the energy shaping in the control input (27) is given as

$$u_{es}=(G^TG)^{-1}G^T(\nabla_q U-M_dM^{-1}\nabla_q U_d)=K_{p1}\tilde{q}_0+K_{p2}\tilde{q}_1 \tag{40}$$

where

$$K_{p1}=\frac{I_t(a_1a_3-a_2^2)}{(-a_2+\varphi'(0)a_1)^2}(K_1(-a_3+\varphi'(0)a_2)+\omega_1^2)$$

$$K_{p2}=\frac{a_1\omega_1^2-K_1(a_1a_3-a_2^2)}{(-a_2+\varphi'(0)a_1)}$$

The controller design is completed with a second term, corresponding to the damping injection. This is achieved via negative feedback of the passive output $G^T\nabla_p H_d$, (24). As

$H_d = (1/2)p^T M_d^{-1} p + U_d(\tilde{q})$, and U_d only depends on the $\tilde{q}$ variable, u_{di} only depends on the appropriate election of M_d :

$$u_{di} = K_{v1}\dot{\tilde{q}}_0 + K_{v2}\dot{\tilde{q}}_1 \tag{41}$$

with

$$K_{v1} = K_v \frac{I_t(-a_3 + \varphi'(0)a_2)}{(a_1 a_3 - a_2^2)}$$
$$K_{v2} = K_v \frac{(a_2 - \varphi'(0)a_1)}{(a_1 a_3 - a_2^2)}$$

A simple analysis on the constants K_{p1} and K_{v1} with the conditions previously imposed, implies that both should be negative to assure the stability of the system.
To analyze the stability of the closed-loop system we consider the energy-based Lyapunov function candidate (Kelly & Campa, 2005), (Sanz & Etxebarria, 2007)

$$\begin{aligned} V(\tilde{q},\dot{\tilde{q}}) = \frac{1}{2}p^T M_d^{-1} p + U_d = \frac{1}{2}\frac{I_t^2\dot{\tilde{q}}_0^2 a_3 - 2I_t\dot{\tilde{q}}_0\dot{\tilde{q}}_1 a_2 + \dot{\tilde{q}}_1^2 a_1}{a_1 a_3 - a_2^2} - \frac{1}{2}\frac{I_t^2\omega_1^2(a_3 - \varphi'(0)a_2)\tilde{q}_0^2}{(-a_2 + \varphi'(0)a_1)^2} \\ - \frac{I_t\omega_1^2\tilde{q}_0\tilde{q}_1}{-a_2 + \varphi'(0)a_1} + \frac{1}{2}K_1(\gamma\tilde{q}_0 + \tilde{q}_1)^2 \end{aligned} \tag{42}$$

which is globally positive definite, i.e: $V(0,0)=(0,0)$ and $V(\tilde{q},\dot{\tilde{q}}) > 0$ for every $(\tilde{q},\dot{\tilde{q}}) \neq (0,0)$.
The time derivative of (42) along the trajectories of the closed-loop system can be written as

$$\dot{V}(\tilde{q},\dot{\tilde{q}}) = -K_v \frac{(I_t\dot{\tilde{q}}_0(-a_3 + \varphi'(0)a_2) + (a_2 - \varphi'(0)a_1)\dot{\tilde{q}}_1)^2}{(a_1 a_3 - a_2^2)^2} \leq 0 \tag{43}$$

where K_v>0, so $\dot{V}$ is negative semidefinite, and $(\tilde{q},\dot{\tilde{q}}) = (0,0)$ is stable (not necessarily asymptotically stable).
By using LaSalle's invariant set theory, it can be defined the set R as the set of points for which $\dot{V} = 0$

$$R = \left\{ \begin{pmatrix} \tilde{q}_0 \\ \tilde{q}_1 \\ \dot{\tilde{q}}_0 \\ \dot{\tilde{q}}_1 \end{pmatrix} \in \mathbb{R}^4 : \dot{V}(\tilde{q},\dot{\tilde{q}}) = 0 \right\} = \left\{ \tilde{q}_0, \tilde{q}_1 \in \mathbb{R}^1 \quad \& \quad \gamma\dot{\tilde{q}}_0 + \dot{\tilde{q}}_1 = 0 \right\} \tag{44}$$

Following LaSalle's principle, given R and defined N as the largest invariant set of R, then all the solutions of the closed loop system asymptotically converge to N when $t \to \infty$.
Any trajectory in R should verify:

$$\gamma\dot{\tilde{q}}_0 + \dot{\tilde{q}}_1 = 0 \tag{45}$$

and therefore it also follows that:

$$\gamma\ddot{\tilde{q}}_0 + \ddot{\tilde{q}}_1 = 0 \tag{46}$$

$$\gamma\tilde{q}_0 + \tilde{q}_1 = k \tag{47}$$

Considering the closed-loop system and the conditions described by (46) and (47), the following expression is obtained:

$$(\frac{\gamma}{I_t} + \varphi'(0) - K_f)k + (\frac{\gamma\omega_1^2}{(-a_2 + \varphi'(0)a_1)} + \varphi'(0))\tilde{q}_0 = 0 \tag{48}$$

As a result of the previous equation, it can be concluded that $\tilde{q}_0(t)$ should be constant, in consequence $\dot{\tilde{q}}_0(t) = 0$, and replacing it in (45), it also follows that $\tilde{q}_1(t) = 0$. Therefore $\ddot{\tilde{q}}_0 = \ddot{\tilde{q}}_1 = 0$ and replacing these in the closed-loop system this leads to the following solution:

$$\begin{pmatrix} \tilde{q}_0(t) \\ \tilde{q}_1(t) \end{pmatrix} = \begin{pmatrix} 0 \\ 0 \end{pmatrix}$$

In other words, the largest invariant set *N* is just the origin $(\tilde{q}, \dot{\tilde{q}}) = (0,0)$, so we can conclude that any trajectory converge to the origin when $t \to \infty$, so the equilibrium is in fact asymptotically stable.

To illustrate the performance of the proposed IDA-PBC controller, in this section we present some simulations. We use the model of a flexible robotic arm presented in (Canudas et al., 1996) and the values of Table 2 which correspond to the real arm displayed in Fig. 9.

The results are shown in Figs. 10 to 12. In these examples the values a_1=1, a_2=0.01 and a_3=50 have been used to complete the conditions (33) and (39). In Fig. 10 the parameters are K_1=10 and K_v=1000. In Figs. 11 and 12 the effect of modifying the damping constant K_v is demonstrated. With a smaller value of K_v, K_v =10, the rigid variable follows the desired trajectory reasonably well. For K_v =1000, the tip position exhibits better tracking of the desired trajectory, as it can be seen comparing Fig. 10(a) and Fig. 11(a). Even more important, it should be noted that the oscillations of elastic modes are now attenuated quickly (compare Fig. 10(c) and Fig. 11(b)). But If we continue increasing the value of K_v, K_v =100000, the oscillations are attenuated even more quickly (compare Fig. 10(c) and Fig. 12(b)), but the tip position exhibits worse tracking of the desired trajectory.

Property	Value
Motor inertia, I_h	0.002 kgm^2
Link length, L	0.45 m
Link height, h	0.02 m
Link thickness, d	0.0008 m
Link mass, M_b	0.06 kg
Linear density, ρ	0.1333 kg/m
Flexural rigidity, EI	0.1621 Nm^2

Table 2. Flexible link parameters

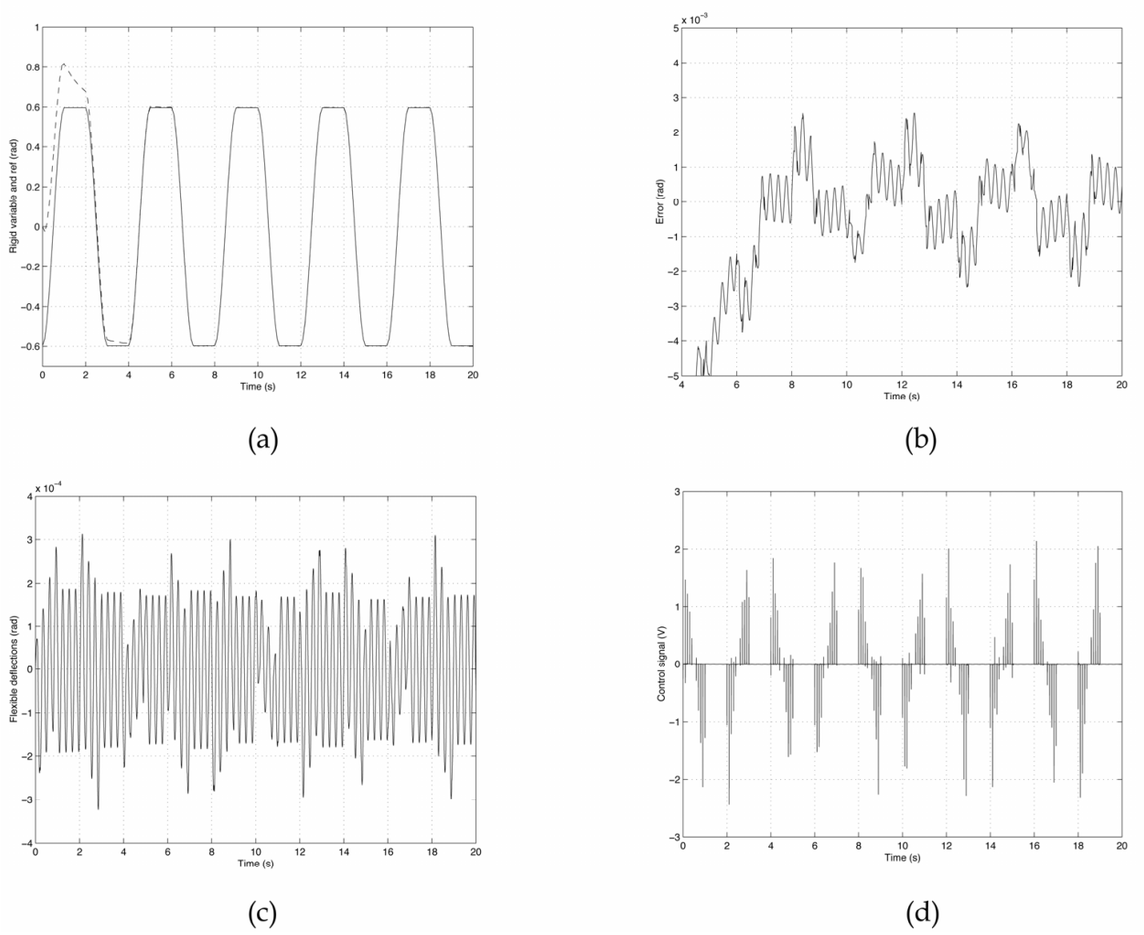

Figure 10. Simulation results for IDA-PBC control with K_v=1000: (a) Time evolution of the rigid variable q_0 and reference q_d__; (b) Rigid variable tracking error; (c) Time evolution of the flexible deflections; (d) Composite control signal

The effectiveness of the proposed control schemes has been tested by means of real time experiments on a laboratory single flexible link. This manipulator arm, fabricated by Quanser Consulting Inc. (Ontario, Canada), is a spring steel bar that moves in the horizontal plane due to the action of a DC motor. A potentiometer measures the angular position of the system, and the arm deflections are measured by means of a strain gauge mounted near its base (see Fig. 9). These sensors provide respectively the values of q_0 and q_1 (and thus $\tilde{q}_0$ and $\tilde{q}_1$ are also known, since q_{0d} and q_{1d} are predetermined).

The experimental results are shown on Figs. 13, 14 and 15. In Fig. 13 the control results using a conventional PD rigid control design are displayed:

$$u = K_P(q_0 - q_{0d}) + K_D(\dot{q}_0 - \dot{q}_{0d})$$

where K_P=-14 and K_D=-0.028. These gains have been carefully chosen, tuning the controller by the usual trial-an-error method. The rigid variable tracks the reference (with a certain error), but the naturally excited flexible deflections are not well damped (Fig. 13(b)).

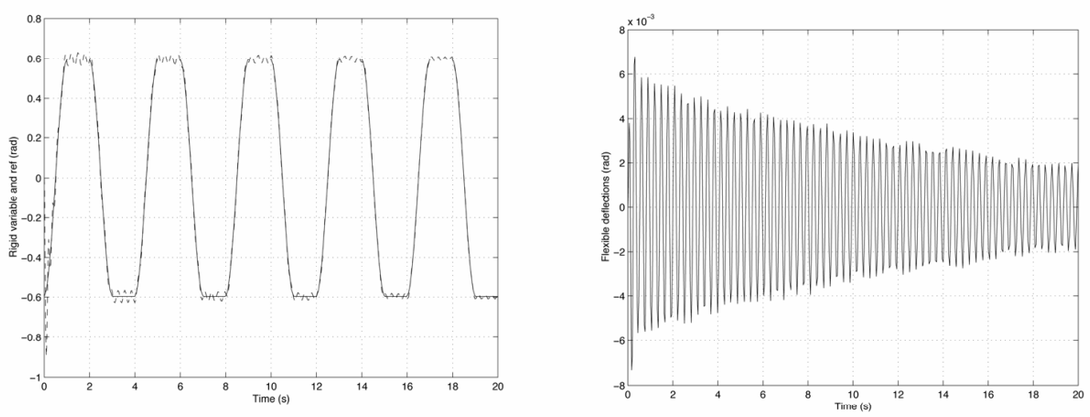

(a) (b)

Figure 11. Simulation results for IDA-PBC control with K_v=10: (a) Time evolution of the rigid variable q_0 and reference q_d__; (b) Time evolution of the flexible deflections

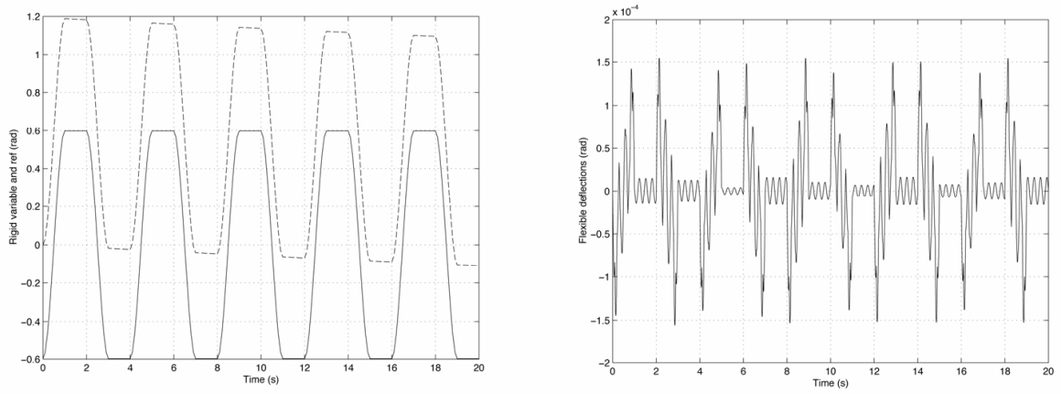

(a) (b)

Figure 12. Simulation results for IDA-PBC control with K_v=100000: (a) Time evolution of the rigid variable q_0 and reference q_d__; (b) Time evolution of the flexible deflections

In Fig. 14 the results using the IDA-PBC design philosophy are displayed. The values a_1=1, a_2=0.01, a_3=50, K_1=10, K_v=1000 and $\varphi'(0) = 1.11$ have been used. As seen in the graphics, the rigid variable follows the desired trajectory, and moreover the flexible modes are now conveniently damped, (compare Fig. 13(b) and Fig. 14(c)). It is shown that vibrations are effectively attenuated in the intervals when q_d reaches its upper and lower values which go from 1 to 2 seconds, 3 to 4 s., 5 to 6 s., etc.

The PD controller might be augmented with a feedback term for link curvature:

$$u = K_P(q_0 - q_{0d}) + K_D(\dot{q}_0 - \dot{q}_{0d}) + K_C \mathrm{w}''$$

where w'' represents the link curvature at the base of the link. This is a much simpler version of the IDA-PBC and doesn't require time derivatives of the strain gauge signals.

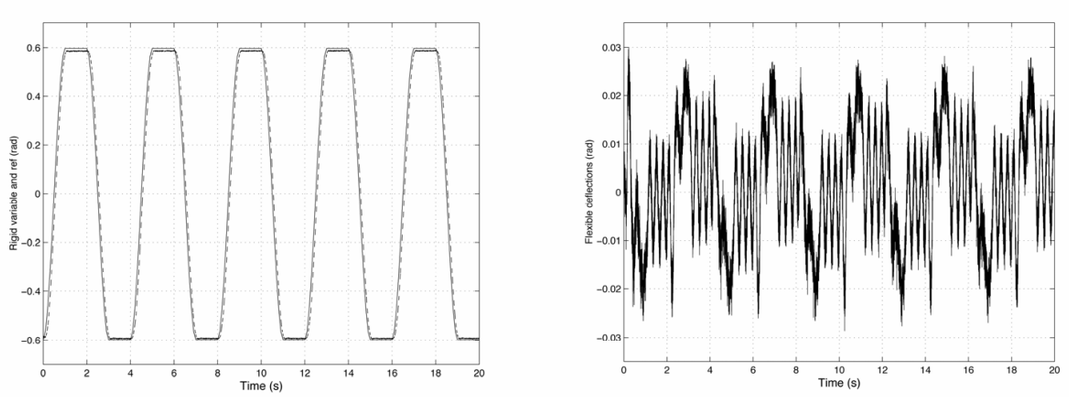

Figure 13. Experimental results for a conventional PD rigid controller:: (a) Time evolution of the rigid variable q_0 and reference q_d__; (b) Time evolution of the flexible deflections

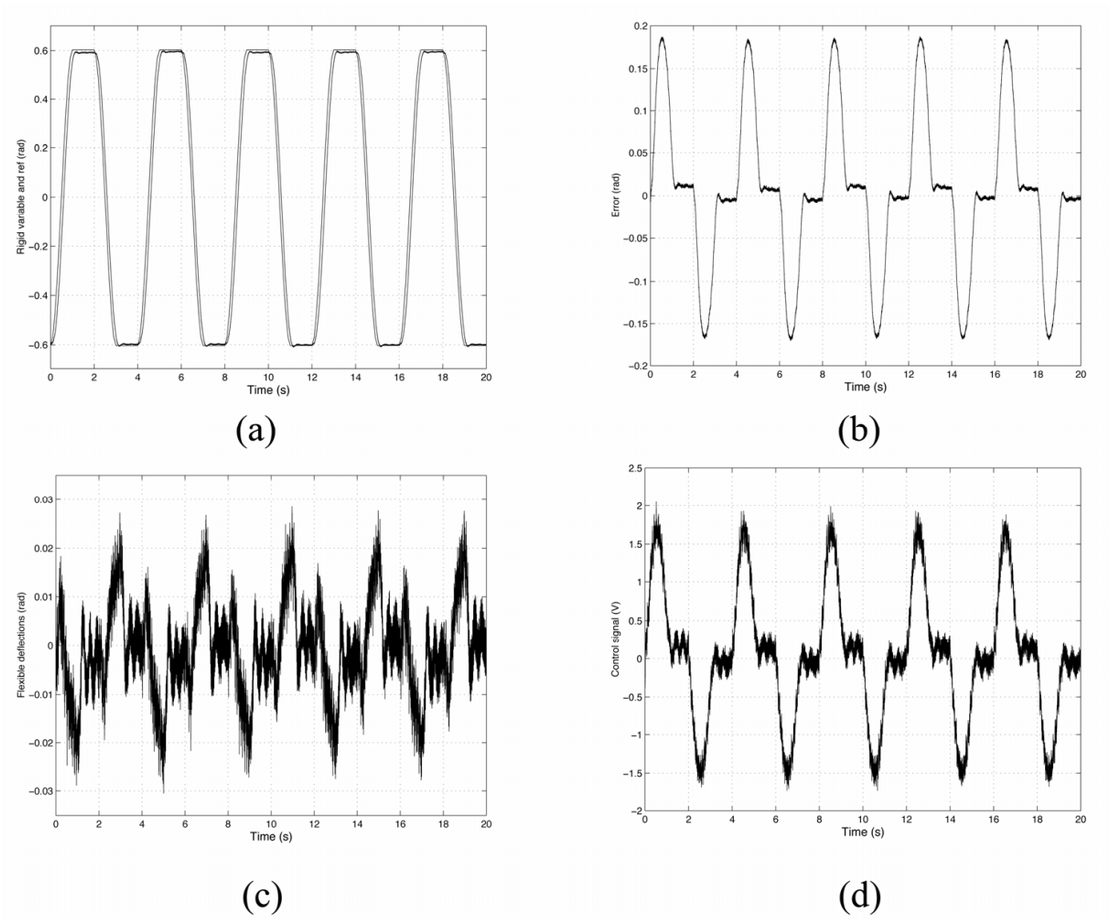

Figure 14. Experimental results for IDA-PBC control: (a) Time evolution of the rigid variable q_0 and reference q_d__; (b) Rigid variable tracking error; (c) Time evolution of the flexible deflections; (d) Composite control signal

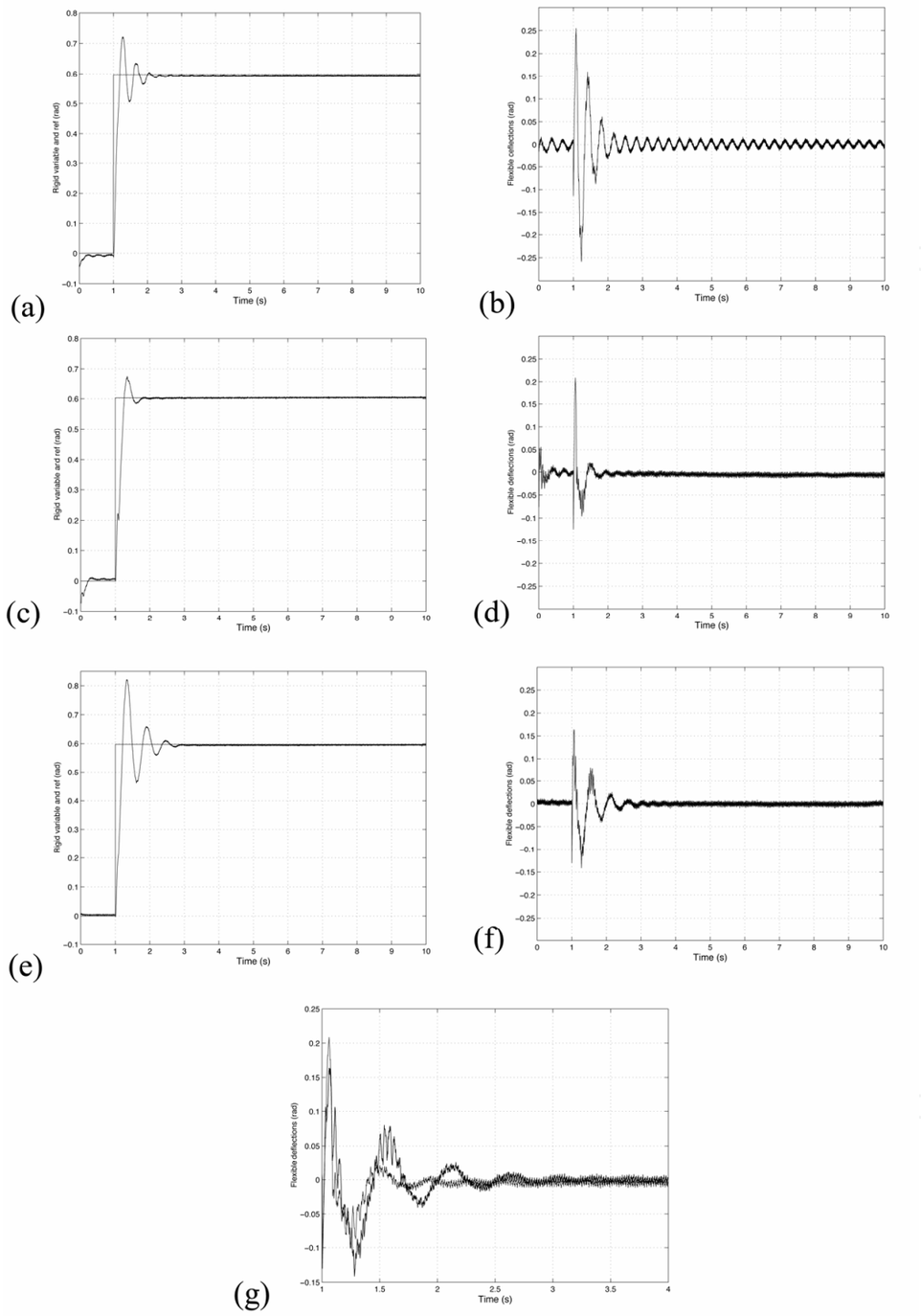

Figure 15. Performance comparison between a conventional rigid PD controller, augmented PD and IDA-PBC controller. (a) Time evolution of the rigid variable q_0 and reference q_d__(PD); (b) Time evolution of the flexible deflections (PD); (c) Time evolution of the rigid variable q_0 and reference q_d__(IDA-PBC); (d) Time evolution of the flexible deflections (IDA-PBC); (e) Time evolution of the rigid variable q_0 and reference q_d__(augmented PD); (f) Time evolution of the flexible deflections (augmented PD); (g) Comparison between the strain gauge signals with the IDA-PBC controller and the augmented PD controller

Fig. 15 shows the comparison between the conventional rigid PD controller, augmented PD and the IDA-PBC controller for a step input. The K_P and K_D gains are the same both for the PD and the augmented PD case. Gain K_C has been carefully tuned to effectively damp the flexible vibrations in the augmented PD control. Comparing Fig. 15(a,b) to Fig. 15(c,d) it is clearly seen how with the IDA-PBC controller the tip oscillation improves notably. Moreover, from Fig. 15(e,f) it can be observed that the augmented PD effectively attenuates the flexible vibrations, but at the price of worsening the rigid tracking. Also in Fig. 15(g), where the flexible responses of both the augmented PD and the IDA-PBC controllers have been amplified and plotted together for comparison, it can be observed that the effective attenuation time is longer in the augmented PD case (2 seconds) than in the IDA-PBC case (1 second).
Notice that the final structure of all the considered controls is similar but with very different gains and all of them imply basically the same implementation effort, although the IDA-PBC gains calculation may imply solving some involved equations. In this sense, the IDA-PBC method gives for this application an energy interpretation of the control gains values and it can be used, in this particular case, as a systematic method for tuning these gains (outperforming the trial-and-error method). Finally, it should be remarked that for a more complicated robot the structure of the IDA-PBC and the PD controls can be very different.

5. Conclusion

An experimental study of several control strategies for flexible manipulators has been presented in this chapter. As a first step, the dynamical model of the system has been derived from a general multi-link flexible formulation. If should be stressed the fact that some simplifications have been made in the modelling process, to keep the model reasonably simple, but, at the same time, complex enough to contain the main rigid and flexible dynamical effects. Three control strategies have been designed and tested on a laboratory two-dof flexible manipulator. The first scheme, based on an LQR optimal philosophy, can be interpreted as a conventional rigid controller. It has been shown that the rigid part of the control performs reasonably well, but the flexible deflections are not well damped. The strategy of a combined optimal rigid-flexible LQR control acting both on the rigid subsystem and on the flexible one has been tested next. The advantage that this type of combined control offers is that the oscillations of the flexible modes attenuate considerably, which demonstrates that a strategy of overlapping a rigid control with a flexible control is effective from an experimental point of view. The third experimented approach introduces a sliding-mode controller. This control includes two completely different parts: one sliding for the rigid subsystem and one LQR for the fast one. In this case the action of the energetic control turns out to be effective for attracting the rigid dynamics to the sliding band, but at the same time the elastic modes are attenuated, even better than in the LQR case. This method has been shown to give a reasonably robust performance if it is conveniently tuned.
The IDA-PBC method is a promising control design tool based on energy concepts. In this chapter we have also presented a theoretical and experimental study of this method for controlling a laboratory single flexible link, valuing in this way the potential of this technique in its application to under-actuated mechanical systems, in particular to flexible manipulators. The study is completed with the Lyapunov stability analysis of the closed-loop system that is obtained with the proposed control law. Then, as an illustration, a set of simulations and laboratory control experiments have been presented. The experimented

scheme, based on an IDA-PBC philosophy, has been shown to achieve good tracking properties on the rigid variable and definitely superior damping of the unwanted vibration of the flexible variables compared to conventional rigid robot control schemes. In view of the obtained experimental results, Fig. 13, 14 and 15, it has also been shown that the proposed IDA-PBC controller leads to a remarkable improvement in the tip oscillation of the robot arm with respect to a conventional PD or an augmented PD approach. It is also worth mentioning that for our application the proposed energy-based methodology, although includes some involved calculations, finally results in a simple controller as easily implementable as a PD. In summary, the experimental results shown in the chapter have illustrated the suitability of the proposed composite control schemes in practical flexible robot control tasks

6. References

O. Barambones and V. Etxebarria, Robust adaptive control for robot manipulators with unmodeled dynamics. *Cybernetics and Systems*, 31(1), 67-86, 2000.

C. Canudas de Wit, B. Siciliano and G. Bastin, Theory of Robot Control. *Europe: The Zodiac*, Springer, 1996.

R. Kelly and R. Campa, Control basado en IDA-PBC del péndulo con rueda inercial: Análisis en formulación lagrangiana. *Revista Iberoamericana de Automática e Informática Industrial*,1, pp. 36--42,January 2005.

P. Kokotovic, H. K. Khalil and J.O'Reilly, *Singular perturbation methods in control*. SIAM Press, 1999.

Y. Li, B. Tang, Z. Zhi and Y. Lu, Experimental study for trajectory tracking of a two-link flexible manipulator. *International Journal of Systems Science*, 31(1):3-9, 2000.

M. Moallem, K. Khorasani and R.V. Patel, Inversion-based sliding control of a flexible-link manipulator. *International Journal of Control*, 71(3), 477-490, 1998.

M. Moallem, R.V. Patel and K. Khorasani, Nonlinear tip-position tracking control of a flexible-link manipulator: theory and experiments. *Automatica*, 37, pp.1825--1834, 2001.

R. Ortega and M. Spong, Stabilization of underactuatedmechanical systems via interconnection and damping assignment, in *Proceedings of the 1st IFAC Workshop on Lagrangian and Hamiltonian methods in nonlinear systems*, Princeton, NJ,USA, 2000, pp. 74--79.

R. Ortega and M. Spong and F. Gómez and G. Blankenstein, Stabilization of underactuated mechanical systems via interconnection and damping assignment. *IEEE Transactions on Automatic Control*, AC-47, pp. 1218--1233, 2002.

R. Ortega and A. van der Schaft and B. Maschke and G. Escobar, Interconnection and damping assignment passivity-based control of port-controlled Hamiltonian systems. *Automatica*, 38, pp. 585--596, 2002.

A. Sanz and V. Etxebarria, Experimental Control of a Two-Dof Flexible Robot Manipulator by Optimal and Sliding Methods. *Journal of Intelligent and Robotic Systems*, 46: 95-110, 2006.

A. Sanz and V. Etxebarria, Experimental control of a single-link flexible robot arm using energy shaping. *International Journal of Systems Science*, 38(1): 61-71, 2007.

M. W. Vandegrift, F. L. Lewis and S. Q. Zhu, Flexible-link robot arm control by a feedback linearization singular perturbation approach. *Journal of Robotic Systems*, 11(7):591-603, 1994.

D. Wang and M. Vidyasagar, Transfer functions for a flexible link. *The International Journal of Robotic Research*, 10(5), pp. 540--549, 1991.

J.X. Xu and W.J. Cao, Direct tip regulation of a single-link flexible manipulator by adaptive variable structure control.*International Journal of Systems Science*, 32(1): 121-135, 2001.

J.H. Yang, F.L. Lian, L.C. Fu, Nonlinear adaptive control for flexible-link manipulators. *IEEE Transactions on Robotics and Automation*, 13(1): 140-148, 1997.

The Mathworks, Inc, Control System Toolbox.*Natick*, MA, 2002.

S. Yoshiki and K. Ogata and Y. Hayakawa, Control of manipulator with 2 flexible-links via energy modification method by using modal properties, in *Proceedings of the 2003 IEEE/ASME International Conference on Advanced Intelligent Mechatronics* (AIM 2003), pp. 1435--1441.

Robot Manipulators

Edited by Marco Ceccarelli

ISBN 978-953-7619-06-0

Hard cover, 546 pages

Publisher InTech

Published online 01, September, 2008

Published in print edition September, 2008

In this book we have grouped contributions in 28 chapters from several authors all around the world on the several aspects and challenges of research and applications of robots with the aim to show the recent advances and problems that still need to be considered for future improvements of robot success in worldwide frames. Each chapter addresses a specific area of modeling, design, and application of robots but with an eye to give an integrated view of what make a robot a unique modern system for many different uses and future potential applications. Main attention has been focused on design issues as thought challenging for improving capabilities and further possibilities of robots for new and old applications, as seen from today technologies and research programs. Thus, great attention has been addressed to control aspects that are strongly evolving also as function of the improvements in robot modeling, sensors, servo-power systems, and informatics. But even other aspects are considered as of fundamental challenge both in design and use of robots with improved performance and capabilities, like for example kinematic design, dynamics, vision integration.

INTECH
open science | open minds

InTech Europe
University Campus STeP Ri
Slavka Krautzeka 83/A
51000 Rijeka, Croatia
Phone: +385 (51) 770 447
Fax: +385 (51) 686 166
www.intechopen.com

InTech China
Unit 405, Office Block, Hotel Equatorial Shanghai
No.65, Yan An Road (West), Shanghai, 200040, China
中国上海市延安西路65号上海国际贵都大饭店办公楼405单元
Phone: +86-21-62489820
Fax: +86-21-62489821

IntechOpen